



## Measurement of capillary pressure in fuel cell diffusion media, micro-porous layers, catalyst layers, and interfaces



Jacob M. LaManna <sup>a</sup>, James V. Bothe Jr. <sup>a</sup>, Feng Yuan Zhang <sup>b</sup>, Matthew M. Mench <sup>a, c, \*</sup>

<sup>a</sup> Department of Mechanical, Aerospace and Biomedical Engineering, The University of Tennessee, Knoxville, TN 37996, USA

<sup>b</sup> Department of Mechanical, Aerospace and Biomedical Engineering, The University of Tennessee Space Institute, Tullahoma, TN 37388, USA

<sup>c</sup> Energy and Transportation Science Division, Oak Ridge National Laboratory, Oak Ridge, TN 37931, USA

### HIGHLIGHTS

- Method of Standard Porosimetry used to determine capillary pressure.
- Experimental high tortuosity diffusion media tested.
- Modified Leverett J-Functions developed.
- Interfacial effects increase pore diameter of MPL when coated on DM.
- Interfacial effects found between MPL and CL caused by voids.

### ARTICLE INFO

#### Article history:

Received 11 March 2014

Received in revised form

8 July 2014

Accepted 22 July 2014

Available online 1 August 2014

#### Keywords:

Leverett

Polymer electrolyte fuel cell

Saturation

Flooding

Capillary

Water management

### ABSTRACT

In this work, semi-empirical Leverett J-Function relationships relating capillary pressure and water saturation are experimentally derived for commercial and experimental polymer electrolyte fuel cell materials developed for automotive applications. Relationships were derived for Mitsubishi Rayon Corp. (MRC) U105 and General Motors (GM) experimental high tortuosity diffusion media (DM), the micro-porous layer (MPL), and the catalyst layer (CL). The standard Leverett J-Function under-predicted drainage curves for the DM at high saturation levels and significantly under-predicted the capillary pressure requirements for the MPL and CL across the entire saturation range. Composite structures were tested to understand interfacial effects for DM|MPL and MPL|CL. Each additional layer was found to superimpose its effects on capillary pressure onto the previous layers. The MPL formulation tested increased in porosity from a 136 nm peak average to a 153 nm peak average with increased surface porosity of the substrate. Additionally, small voids and pockets that accumulate liquid water were found to exist in the MPL|CL interface. The results of this work are useful for computational modelers seeking to enhance the resolution of their macroscopic multi-phase flow models which underestimate capillary pressure using the standard Leverett J-Function.

© 2014 Elsevier B.V. All rights reserved.

### 1. Introduction

Multi-phase flow in polymer electrolyte fuel cells (PEFCs) impacts instantaneous performance, operational stability, and long-term and freeze durability [1–14]. It is well established that the addition of a micro-porous layer (MPL) to the macro diffusion media (DM) results in enhanced performance of PEFCs via

improved water management and interfacial contact [15–18]. A portion of these studies focus on just the physical properties of the MPL, DM, or other porous layers themselves, but often this cannot explain experimentally observed phenomena. A study by Ramasamy et al. [15] shows how different combinations of MPL and DM under wet and dry conditions result in varied performance outcomes. On the anode, the MPL can help prevent evaporative removal and dry-out, and at the cathode an MPL can prevent the onset of flooding losses. Thus, an asymmetric DM arrangement between the anode and cathode can be beneficial.

Clearly, it is critical to understand and quantify capillary flow in the various porous media as a function of engineering parameters. Additionally, to gain a more detailed understanding of two-phase

\* Corresponding author. Department of Mechanical, Aerospace and Biomedical Engineering, The University of Tennessee, Knoxville, TN 37996, USA. Tel.: +1 865 974 6751; fax: +1 865 974 5274.

E-mail address: [mmench@utk.edu](mailto:mmench@utk.edu) (M.M. Mench).

mass transport through a bi-layered diffusion media, it is desirable to understand the interfacial region between the MPL and DM, or the MPL and the catalyst layer (CL), where recent work has suggested a strong influence on PEFC performance [19–21]. Hizir et al. [19] investigated the influence of interfacial morphology and showed a high degree of surface roughness and micro-cracks on the surfaces of MPL and CL which provide sites for possible water accumulation and increased mass transfer losses. Utilizing these results, a modeling study by Bajpai et al. [20] simulated performance losses expected when voids, either filled with water vapor or liquid water, are present at the CL|MPL interface. Swamy et al. [21] developed a 2-dimensional computational model to simulate the interfacial compression and morphology of MPL and CL surfaces.

Experimental results taken using neutron imaging have shown evidence of interfacial water accumulation along the CL|MPL interface [22,23]. Additional evidence of interfacial accumulation of liquid based on X-ray studies show an accumulation of liquid in the MPL|DM interfacial region [24]. Recently, Manahan et al. has shown new evidence pointing to interfacial effects [25,26] using MPL|DM composites with laser-based perforations. The neutron imaging based results of Turhan et al. [27] conclusively demonstrate that the abrupt change in saturation predicted by conventional domain-based computational models [28] does not exist, and instead another explanation for the observed internal distribution profile is needed. Preston et al. [29] suggested that interpenetration between the MPL and DM results in a more gradual change in properties along the interfacial region than predicted by conventional modeling. Phase change induced flow has also been investigated, and found to contribute to and in some cases govern the resulting internal water distribution observed experimentally [30–33].

Nam et al. [34] used mathematical modeling and an environmental SEM to simulate the breakthrough of liquid water droplets in porous media such as CL, MPL, and DM. Their findings suggest that the very fine porosity of the CL nucleates a large number of water droplets at the interface that coalesce and fill the large pores of the adjacent DM, thereby inducing flooding. However, inserting a MPL of optimum thickness and having a graded pore structure can effectively reduce water saturation at both the CL|MPL and MPL|DM interfaces.

In porous media, capillary pressure ( $P_c$ ) is strongly correlated to water saturation ( $s_{nw}$ ). In turn, the saturation in the DM, MPL, and CL can be related to various polarization losses through established relationships. The relationship between the two parameters is therefore essential for modelers addressing water management issues in PEFCs. Nearly all macroscopic multi-phase models published to date have relied on the Leverett-based approach with J-function [35], as defined by the following equation:

$$J(s_{nw}) = \frac{P_c(\text{water-air})}{\sigma \cos \theta} \left[ \frac{k}{\epsilon} \right]^{1/2} \quad (1)$$

where  $\sigma$  is the liquid-air surface tension of the working fluid,  $\theta$  is the contact angle,  $k$  is the permeability of the porous substrate, and  $\epsilon$  its porosity. It should be noted that this relationship is based on semi-empirical formulations derived originally from soil science, and thus are only expected to qualitatively explain bulk capillary behavior in thin-film fuel cell porous media, and not microscopic surface coverage or interfacial behavior in the various media [36]. For example, flooding in the CL can occur as a result of extremely low levels of effective saturation through thin layer coverage of the catalyst surface.

Recently, Çeçen et al. [37] and Wargo et al. [38,39] have developed methods for characterization of certain relevant porous media properties such as tortuosity based on microstructure analysis. This

type of work promises to relate specific microstructure properties to operational performance in the future, and goes a step beyond the bulk flow relationships derived here. However, for the purposes of classical multi-phase flow simulation and computational tractability, bulk material flow relationships are still quite useful. Thus, the work here is between microscale levels of localized characterization and generic bulk flow approximations that have been identified to have significant error, and seeks to develop material-specific capillary pressure–saturation relationships used in modeling and simulation.

Gostick et al. [40] plotted  $P_c-s_{nw}$  data for certain diffusion media, both untreated hydrophilic and polytetrafluoroethylene (PTFE) treated hydrophobic, as well as woven cloth types, as a function of the Leverett J-function defined in Eq. (1). Their study showed that the data from the different materials fall reasonably well on a single curve. Kumbur et al. [41–43] also utilized the Leverett-based approach, but to derive a series of equations to fit their experimentally determined  $P_c-s_{nw}$  data as a function of temperature, compression pressure, and hydrophobicity of the diffusion media. Their data were extracted from bi-layered composite systems, rather than from individual porous substrate layers. Their results indicated that a significant error in predicted  $P_c$  values for a given saturation can occur if using the standard Leverett function. Specifically, the standard function will significantly underestimate the capillary pressure at a given saturation. According to Preston [29], and Gostick [40], using a Leverett-based approach can prove to be useful in modeling  $P_c-s_{nw}$  data from single-layered porous substrates, but cannot differentiate the contributions from each individual porous layer in a multi-layered composite structure, such as MPL|DM.

This study is motivated by the need to deduce individual capillary pressure versus saturation relationships for the MPL and CL as separate porous substrates, as well as investigate the impact of interfaces between mating layers on the individualized component measurement. Accordingly,  $P_c-s_{nw}$  data were collected from individual and commercially available MPL, DM, and CL materials, as well as the MPL|DM and CL|MPL|DM composites for comparison. The results of this work should also be useful for computational modelers seeking to enhance the resolution of their macroscopic multi-phase flow models.

## 2. Experimental procedure

### 2.1. Measurement methodology

The Method of Standard Porosimetry, MSP, was used to generate the data analyzed in the present study and was measured by MPM&P Research Inc., (formally Porotech, Ltd) of Ontario, Canada. This method is advantageous to the more commonly used method of mercury intrusion porosimetry (MIP) due to the significantly lower pressures required for analysis (MIP can require thousands of atmospheres of pressure) which reduces the likelihood of deformation and damage to the sample. Details of this technique are described at length elsewhere [41,44]. The basic concept entails placing the porous sample of interest into capillary equilibrium with two well characterized porous standards with known  $P_c-s_w$  relationship having a pore-size approximating that of the sample. Once capillary equilibrium among the porous media has been established, measurements are taken by removing and weighing the sample to determine saturation. This procedure is repeated with increasingly lower saturation via evaporation by a flowing dry gas stream until an adequate number of  $P_c-s_w$  data points are generated. The data therefore represent capillary drainage curves for the particular porous medium. The working fluids used were octane, that wets both treated and un-treated carbon surfaces of the porous media, and water, which wets only hydrophilic pores.

Since measurements were taken using fluids that are wetting on pore surfaces of interest, the contact angle can be assumed to be zero. This reduces the Young–Laplace equation to:

$$P_c = \frac{2\sigma}{r} \quad (2)$$

where  $\sigma$  is the surface tension of the working fluid, and  $r$  is the pore radius. To transform data from octane-air capillary pressure to water–air capillary pressure, and then to convert wetting phase saturation to non-wetting phase saturation, the following relationships were used:

$$P_{c(\text{water-air})} = [\sigma_{\text{water}}/\sigma_{\text{octane}}] P_{c(\text{octane-air})} \quad (3)$$

$$s_{nw} = 1 - s_w \quad (4)$$

The result is a series of  $P_c$ – $s_{nw}$  data points that can be plotted in a way that best describes capillary-based water flow through the semi-hydrophobic porous thin film media. All measurements were taken with the porous media under 0.1 MPa of compression pressure.

## 2.2. Materials tested

The commercially available DM tested in this work is Mitsubishi Rayon Corporation (MRC) U105 with 5% PTFE by weight and thickness of 210 µm without MPL and 230 µm with an MPL. The MPL has 8:1:1 carbon to PTFE to fluorinated ethylene propylene (FEP) ratio and approximately 30 µm thickness when coated on the DM. The CL was supplied by General Motors. It was necessary to coat the MPL and CL layers onto non-porous, unreactive polyimide film to test the properties of the layers individually, as it was not possible to produce stand-alone layers. Fig. 1 shows the combinations with which the different materials were tested to determine individual layer and composite material properties.

GM provided an experimental high tortuosity DM to be tested with this work, referred to as GM Exp throughout this paper. This material is constructed of graphite fibers, large graphite flakes, and graphite powder. The graphite flakes are oriented in-plane to produce long path lengths for diffusion, as shown in Fig. 2, to increase the  $D/D_{\text{eff}}$  from 2.8 for the MRC to 19 [45]. Increased diffusion resistance has been identified as a means to reduce anode water content and dry-out for automotive fuel cells. Full details of this material are available in the US patent No. 8518596 [45].

## 2.3. The Leverett J-Function

Traditionally, the Leverett approach with J-function was proposed by Leverett [35] and Udell [46] to describe capillary pressure

in consolidated soil beds of uniform wettability. For hydrophobic media, the standard J-function is described by:

$$J(s_{nw}) = 1.417 s_{nw} - 2.120 s_{nw}^2 + 1.263 s_{nw}^3 \quad (5)$$

the coefficients of which were derived empirically to best fit their soil data. However, fuel cell media tend to be more anisotropic in wettability and for a variety of other reasons described in Ref. [36], the traditional or standard J-function as expressed in Eq. (5) may not be suitable. This was the impetus behind studies by Kumbur et al. [41–43], in which expressions for capillary pressure for fuel cell DM were derived as a function of temperature, PTFE content and compressive pressure. The present study develops a modified J-function of the  $P_c$ – $s_{nw}$  data of the materials tested within a saturation range encompassing normal fuel cell operation.

## 3. Results and discussion

### 3.1. Development of modified Leverett J-Functions

Drainage curves were constructed from the raw data acquired via the MSP. At 100% octane saturation ( $s_w = 1$ ), capillary pressure is at a minimum and increases as all-wetting octane is evaporated and replaced by air from within the porous structure. Capillary pressure rises sharply when the octane-wet porous material is brought to irreducible or connate saturation, where residual octane remains primarily as a continuous phase covering pore walls. In terms of the more relevant water–air system, the same data shows that increasing non-wetting water saturation ( $s_{nw}$ ) simulates water infiltrating into increasingly finer hydrophobic pores with an attendant increase in capillary pressure. Based on extensive measurement using neutron imaging [22,23,25–27,29,47], water saturation from dry to approximately  $s_{nw} = 0.8$  is more than adequate to describe the complete practical range of fuel cell operation, considering that normal fuel cell operation occurs well within a saturation range of  $0 < s_{nw} < 0.6$ .

Modified Leverett J-Functions have been fitted to the experimental MSP data for the MRC DM and the GM Exp DM in Fig. 3 along with the standard Leverett J-Function for comparison. The modified Leverett J-Functions for the relationship of capillary pressure,  $P_c$ , and non-wetting phase saturation,  $s_{nw}$ , have the form:

$$P_c = \sigma \left( \frac{\epsilon}{\kappa} \right)^{1/2} (as_{nw}^3 + bs_{nw}^2 + cs_{nw}) + d \quad (6)$$

where  $\sigma$  is surface tension,  $\epsilon$  is porosity,  $\kappa$  is permeability, and  $a$ ,  $b$ ,  $c$ , and  $d$  represent the coefficients for the fit. Values for these material properties and fitting coefficients are located in Table 1. The valid ranges for the fits are  $0.22 \leq s_{nw} \leq 0.86$  for MRC DM and  $0 \leq s_{nw} \leq 0.58$  for the GM Exp DM. The third-order polynomial form

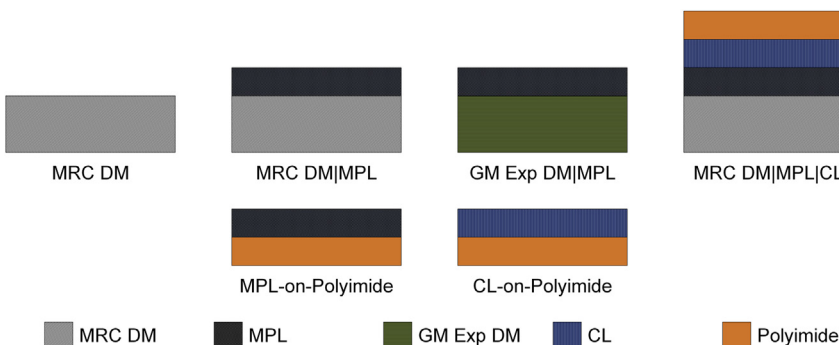


**Fig. 1.** Configuration of materials tested with the Method of Standard Porosimetry (Not to scale).

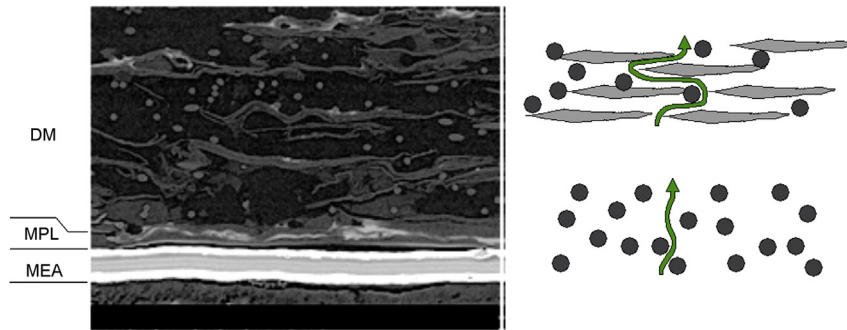


**Fig. 2.** SEM of cross-section of GM experimental high tortuosity DM (left) [45] and schematic of diffusion length for GM experimental high tortuosity DM (top right) versus standard DM (bottom right).

of the modified Leverett J-Function was not capable of capturing the sharp rise in capillary pressure for low saturation values for the MRC DM. To address this issue, a new empirical form of modified Leverett J-Function is proposed for low values of saturation for the MRC DM in the range of  $0 \leq s_{nw} < 0.22$  in Eq. (7) below.

$$P_c = 0.0009 \sigma \left( \frac{\epsilon}{k} \right)^{1/2} s_{nw}^{0.0691} \quad (7)$$

Both the MRC and GM Exp DM show strong deviation from the standard Leverett J-Function for all saturation values. The GM Exp DM requires small increases in pressure to drive large increases in saturation after the initial rise in capillary pressure. Neutron imaging work by LaManna et al. [48] has shown high anode water content that can approach 50% or more for designs with large land-to-channel width ratios. This level of water could make the GM Exp DM more susceptible to flooding than the MRC DM as the lower capillary pressure of drainage in the material could allow rapid spreading of water.

To determine the morphological causes for the difference in drainage profiles it is necessary to examine pore structure differences. Differential pore distribution for the two materials is shown in Fig. 4. The MRC DM (macro side of Fig. 4) has two primary peaks at 6 μm and 27 μm pore diameters, and an average pore diameter of 16 μm. The GM Exp DM begins a slow rise at 2 μm to a single peak at 25 μm diameter, with an average pore diameter of 23 μm. Maximum pore diameter for the MRC DM is 44 μm, while the GM Exp DM has pore diameters that extend out to 286 μm. The per unit area total pore volume for the two samples is 0.01513 and

0.02198 cm<sup>3</sup> cm<sup>-2</sup> for MRC DM and GM Exp DM, respectively. The high volume of large pores and the larger volume per unit area pore volume are the primary contributors to the low capillary pressure observed for the GM Exp DM up to 55% saturation. Once the large pores are filled, pressure requirements to drive water into the smaller pores of the DM increase sharply, as evidenced by the inflection of the GM Exp DM drainage curve (Fig. 3) beyond 55% saturation.

Drainage curves for the Polyimide backed MPL and CL are plotted in Fig. 5 with corresponding fitted modified Leverett J-Functions and the standard Leverett J-Function for comparison. The much smaller pore sizes of the two layers significantly increase the required capillary pressure by nearly 4 orders of magnitude. The modified Leverett J-Functions for the MPL, valid from  $0 \leq s_{nw} \leq 0.82$ , and CL, valid from  $0 \leq s_{nw} \leq 0.68$ , follow the same form as shown in Eq. (6) with the variables and fitting coefficients found in Table 1. In this case the standard Leverett J-function severely underestimates the capillary pressure relationship for the two layers. This is an important finding as models that use the standard Leverett J-Function may predict liquid water flow through the layers at much lower pressures than is actually possible, thus underestimating steady state water accumulation.

As is expected, the CL requires higher pressure to achieve the same saturation as the MPL due to the smaller average pore diameter of 40 nm for the CL to the 81 nm average diameter for the MPL. The total differential pore distributions for the two materials are shown in Fig. 6 with the MPL having nearly twice the pore volume as the CL. Pore distributions for both materials begin at approximately 4 nm diameter and extend to 670 nm for the CL and 6 μm for the MPL. The largest pores in the MPL distribution could possibly be due to small imperfections or cracks in the material.

### 3.2. Interfacial interactions

The second part of this study utilized the MSP data to detect any interfacial behavior as a result of bringing two porous layers together to form a bi-layered porous composite, such as the

**Table 1**  
Property values and fitting coefficients for modified Leverett J-Functions.

Layer	Porosity $\epsilon$	Permeability $k \times 10^{12}$ [m <sup>2</sup> ]	a	b	c	d
MRC DM	0.77	25 [49]	0.00013	0.00482	-0.00026	8
GM Exp DM	0.81	25 [49]	0.02155	-0.02325	0.00798	0
MPL	0.54	0.1 [50]	0.75079	-0.61131	0.17688	0
CL	0.43	0.1 [50]	3.02343	-2.35638	0.55602	0
Octane		Water				
Surface tension $\sigma$ [N m <sup>-1</sup> ]	0.02175	0.07250				

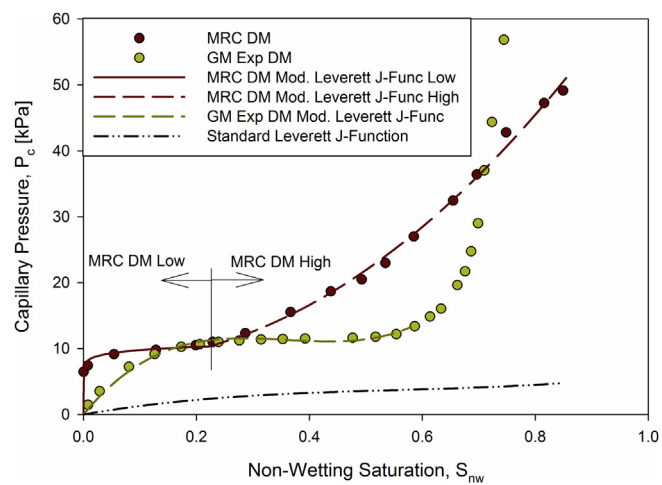


**Fig. 3.** Experimental data for MRC and GM Exp DM with fitted modified Leverett J-Functions compared to standard Leverett J-Function.

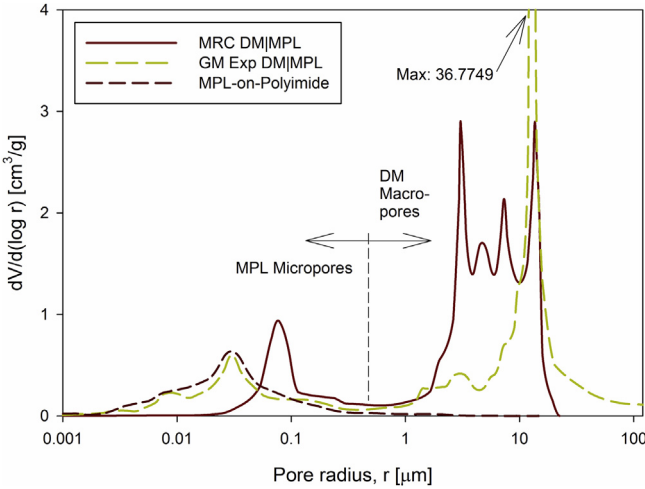


**Fig. 4.** Total differential porosity for MRC DM with MPL, GM Exp with MPL, and MPL-on-Polyimide.

DM|MPL interface. The two composite structures of interest in this work are the MRC DM|MPL and the MRC DM|MPL|CL combinations. Drainage curves for the MRC DM and two composites are plotted in Fig. 7(a). It can be seen that all three profiles overlay each other very well with the initial saturation up to ~75% saturation. At this point, the two composite materials require a sharp increase in capillary pressure to continue imbibition. As it aligns with both composite cases, this initial step change can be attributed to the filling of all macro pores in the DM before the change and the micro pores filling after the step change. Fig. 7(b) represents the area highlighted with the red box in Fig. 7(a) (online) to show better detail of the influence of the CL. The deviation of the MRC DM|MPL|CL profile from the MRC DM|MPL profile shows that the CL acts as another superimposed layer in the composite. The step change from MPL to CL is not as significant as the DM to MPL step because the pore distribution is not as mismatched as the DM|MPL case.

To further investigate interfacial effects between layers in the composite, each interface was probed closer. The MPL portions of the profiles for the MRC DM|MPL and GM Exp DM|MPL from 100 to 100,000 kPa are scaled to align with the MPL-on-Polyimide and are plotted in Fig. 8. This plot shows a significant deviation of the MRC DM|MPL from the other two curves. The sharp rise in saturation versus the more gentle increase for the GM Exp DM|MPL and MPL-

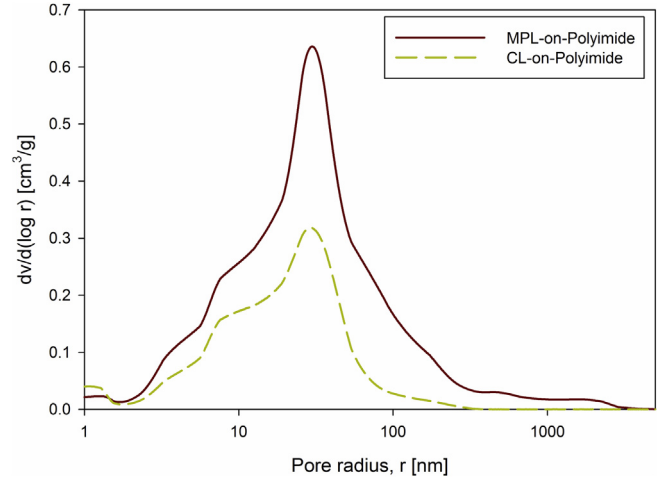


**Fig. 6.** Total differential pore distributions for MPL-on-Polyimide and CL-on-Polyimide.

on-Polyimide indicates a larger pore distribution of the MRC DM|MPL. This increase in pore distribution is corroborated by the differential pore distributions in Fig. 4, showing a shift in the MPL peak for MRC DM|MPL from an 39.6 nm average radius to 97.9 nm. The peak also increases in maximum volume while shrinking the

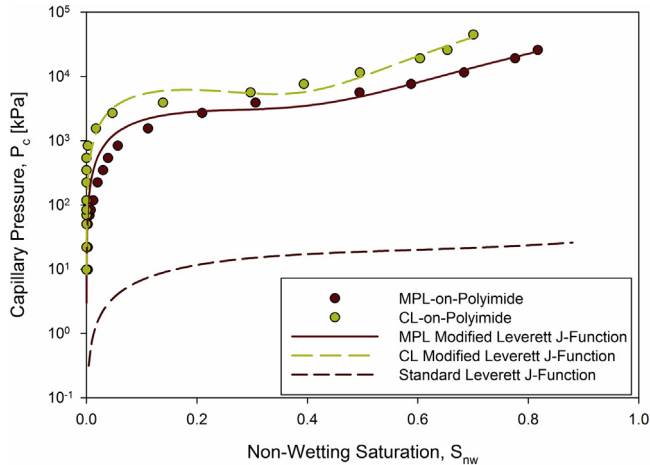
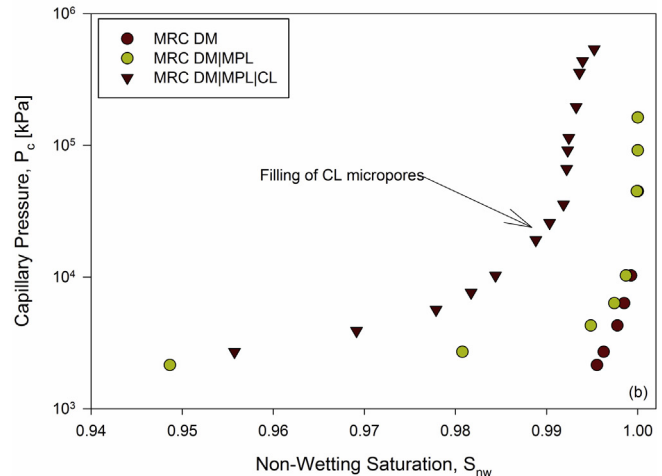
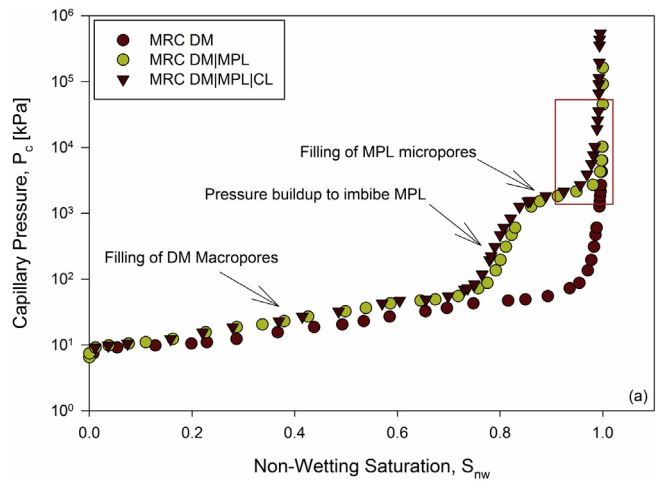


**Fig. 5.** MSP experimental data and fitted modified Leverett J-Functions for MPL-on-Polyimide and CL-on-Polyimide compared to standard Leverett J-Function.

**Fig. 7.** Drainage curves for MRC DM, MRC DM with MPL, and MRC DM|MPL|CL over entire pressure range of MSP test (a) and over range highlighted by box (b).

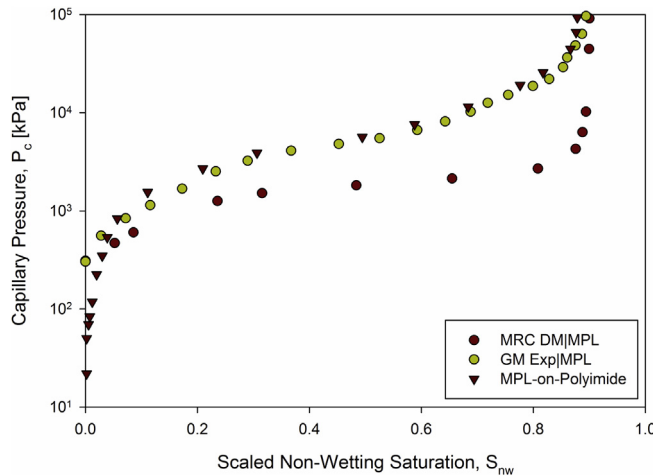


**Fig. 8.** Scaled comparison of MPL interaction showing interfacial influences between porous macro-layer and MPL coating.

width of the peak with an overall reduction in total pore volume of  $0.499 \text{ cm}^3 \text{ g}^{-1}$  for the MPL-on-Polyimide to  $0.329 \text{ cm}^3 \text{ g}^{-1}$  for the MRC MPL. Coating of the MPL onto the MRC DM changes the way the dispersion creates the layer due to the high surface porosity of the MRC DM compared to the non-porous Polyimide surface and the low surface porosity of the GM Exp DM. The large graphite flakes of the GM Exp DM reduce the surface porosity (shown in Fig. 9) and act as non-porous restrictions to the MPL dispersion. This shows the need to properly formulate the MPL dispersion for the particular material that will be coated as future DM may vary significantly from the standard carbon fiber paper typically used in fuel cells.

Scaled profiles of the CL-on-Polyimide and CL influenced zone of the MRC DM|MPL|CL composite are plotted in Fig. 10 to determine if interfacial effects exist in the composite material. The composite profile shows a sharper increase in saturation compared to the CL-on-Polyimide indicating interfacial influence. Since the CL is identical between cases, manufacturing/processing differences between the cases are doubtful. The CL is applied to the MRC DM|MPL by adding a disk of CL-on-Polyimide by pressing it together in the MSP tester. Since the layer was not coated or hot-pressed to increase adhesion to the MPL the integrity of the interface is questionable. The sharper increase in saturation for the composite versus the CL-on-Polyimide could be due to voids and pockets forming between the MPL|CL interface. Experimental neutron imaging results of Manahan and Mench show evidence of liquid accumulation along this interface [26]. Thus, processing and bonding of the individual surfaces can likely mitigate interfacial accumulation and storage issues.

#### 4. Conclusions

Using the Method of Standard Porosimetry (MSP), semi-empirical Leverett function relationships relating capillary pressure to water saturation were deduced for a commercially available and experimental diffusion medium, micro-porous layer, and catalyst layer as stand-alone layers. The GM experimental high tortuosity DM was found to retain water at lower capillary pressures than the commercially available MRC DM. The larger average pore diameter and large pore volume of the experimental DM contributed to reduced capillary pressure required for motion of water. The modified Leverett J-Function for the MRC DM was found to deviate from the standard Leverett J-Function for all saturation values. Extremely high capillary pressure for moderate levels of saturation in the MPL and CL were found, which is expected due to hydrophobic nature and

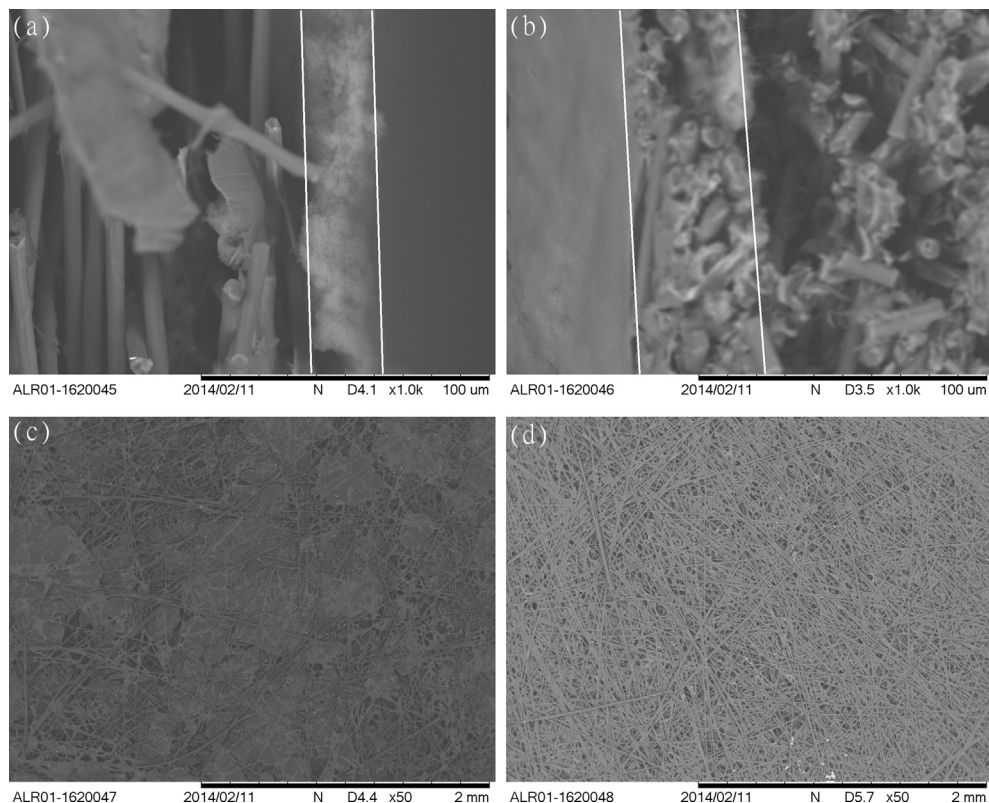


**Fig. 9.** SEM images of the cross-section of the materials shows how the MPL (between white lines) forms a more discrete layer with the GM Exp DM (a) than in the MRC DM (b), in-plane images of the macroporous layers are shown for GM Exp DM (c) and MRC DM (d).

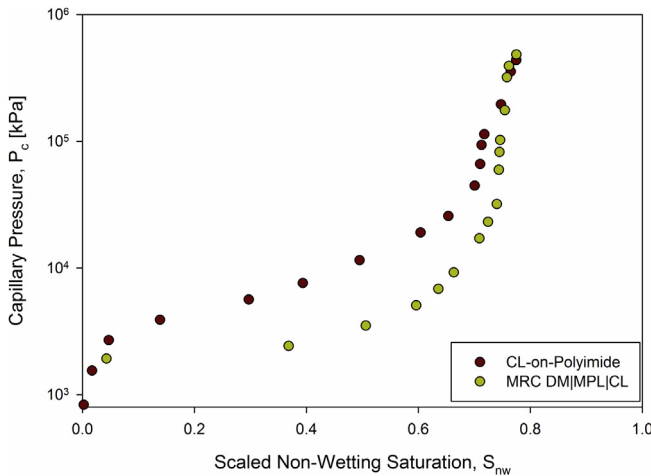


**Fig. 10.** Scaled comparison of catalyst interfacial interaction.

pore size. The standard Leverett J-Function was found to under-predict capillary pressure for the MPL and CL by up to four orders of magnitude. It is therefore not expected that any significant accumulation of liquid in the CL or MPL beyond isolated condensed droplets should exist for extended periods of time during PEFC operation.

Additionally, composite structures were used to determine interfacial effects between the MPL, DM, and CL. The MPL pore structure and pore size distribution was found to be affected by the surface porosity of the material it was coated on with more porous materials, such as the MRC DM, producing a larger pore structure in the MPL. Interfacial water accumulation was found to occur between the MPL and CL in the composite tested in this work. Interfacial effects arose primarily due to the fact that the catalyst layer was not directly coated or hot-pressed to the MPL which allows for the development of voids and pockets for water accumulation. This work highlights the importance of properly engineering the layers to interface with each other to reduce interfacial transport restrictions and liquid water accumulation.

## Disclaimer

This report was prepared as an account of work sponsored by an agency of the United States Government. Neither the United States Government nor any agency thereof, nor any of their employees, makes any warranty, express or implied, or assumes any legal liability or responsibility for the accuracy, completeness, or usefulness of any information, apparatus, product, or process disclosed, or represents that use would not infringe privately owned rights. Reference herein to any specific commercial product, process, or service by trade name, trademark, manufacturer, or otherwise, does not necessarily constitute or imply its endorsement, recommendation, or favoring by the United States Government or any agency thereof. The views and opinions of authors expressed herein do not necessarily state or reflect those of the United States Government or any agency thereof.

## Acknowledgments

This work is funded by the United States Department of Energy Office of Energy Efficiency and Renewable Energy (EERE) under contract number DE-EE0000470. The authors also wish to thank Jon Owejan and Paul Nicotera of General Motors for their support with this ongoing work and supply of materials used for testing.

## References

- [1] M.M. Mench, Fuel Cell Engines, 2008.
- [2] M.M. Mench, E.C. Kumbur, T.N. Veziroglu, Polymer Electrolyte Fuel Cell Degradation, Elsevier, New York, 2012.
- [3] R. Lin, C. Cao, J. Ma, E. GÜLZOW, K. Andreas Friedrich, Int. J. Hydrogen Energy 37 (2012) 3373–3381.
- [4] J.P. Owejan, J.J. Gagliardo, J.M. Sergi, S.G. Kandlikar, T.A. Trabold, Int. J. Hydrogen Energy 34 (2009) 3436–3444.
- [5] K. Jiao, X. Li, Prog. Energy Combust. Sci. 37 (2011) 221–291.
- [6] E.C. Kumbur, M.M. Mench, in: G. Jürgen (Ed.), Encyclopedia of Electrochemical Power Sources, Elsevier, Amsterdam, 2009, pp. 828–847.
- [7] S. Kim, M. Khandelwal, C. Chacko, M.M. Mench, J. Electrochem. Soc. 156 (2009) B99–B108.
- [8] C. Chacko, R. Ramasamy, S. Kim, M. Khandelwal, M. Mench, J. Electrochem. Soc. 155 (2008) B1145–B1154.
- [9] S. Kim, B.K. Ahn, M.M. Mench, J. Power Sources 179 (2008) 140–146.
- [10] S. Kim, M.M. Mench, J. Power Sources 174 (2007) 206–220.
- [11] M. Khandelwal, S. Lee, M.M. Mench, J. Power Sources 172 (2007) 816–830.
- [12] S. He, M.M. Mench, J. Electrochem. Soc. 153 (2006) A1724–A1731.
- [13] S. He, S.H. Kim, M.M. Mench, J. Electrochem. Soc. 154 (2007) B1024–B1033.
- [14] S. He, J.H. Lee, M.M. Mench, J. Electrochem. Soc. 154 (2007) B1227–B1236.
- [15] R.P. Ramasamy, E.C. Kumbur, M.M. Mench, W. Liu, D. Moore, M. Murthy, Int. J. Hydrogen Energy 33 (2008) 3351–3367.
- [16] Z. Qi, A. Kaufman, J. Power Sources 109 (2002) 38–46.
- [17] D. Sernjak, A.K. Prasad, S.G. Advani, J. Power Sources 170 (2007) 334–344.
- [18] M. Blanco, D.P. Wilkinson, H. Wang, Int. J. Hydrogen Energy 36 (2011) 3635–3648.
- [19] F.E. Hizir, S.O. Ural, E.C. Kumbur, M.M. Mench, J. Power Sources 195 (2010) 3463–3471.
- [20] H. Bajpai, M. Khandelwal, E.C. Kumbur, M.M. Mench, J. Power Sources 195 (2010) 4196–4205.
- [21] T. Swamy, E.C. Kumbur, M.M. Mench, J. Electrochem. Soc. 157 (2010) B77–B85.
- [22] M.C. Hatzell, A. Turhan, S. Kim, D.S. Hussey, D.L. Jacobson, M.M. Mench, J. Electrochem. Soc. 158 (2011) B717–B726.
- [23] K.T. Cho, M.M. Mench, Phys. Chem. Chem. Phys. 14 (2012) 4296–4302.
- [24] C. Hartnig, I. Manke, R. Kuhn, N. Kardjilov, J. Banhart, W. Lehnert, Appl. Phys. Lett. 92 (2008) 134106–1–134106–3.
- [25] M.P. Manahan, M.C. Hatzell, E.C. Kumbur, M.M. Mench, J. Power Sources 196 (2011) 5573–5582.
- [26] M.P. Manahan, M.M. Mench, J. Electrochem. Soc. 159 (2012) F322–F330.
- [27] A. Turhan, S. Kim, M. Hatzell, M.M. Mench, Electrochim. Acta 55 (2010) 2734–2745.
- [28] U. Pasaogullari, C.-Y. Wang, Electrochim. Acta 49 (2004) 4359–4369.
- [29] J.S. Preston, R.S. Fu, U. Pasaogullari, D.S. Hussey, D.L. Jacobson, J. Electrochim. Soc. 158 (2011) B239–B246.
- [30] A.Z. Weber, M.A. Hickner, Electrochim. Acta 53 (2008) 7668–7674.
- [31] S. Kim, M.M. Mench, J. Electrochim. Soc. 156 (2009) B353–B362.
- [32] S. Kim, M.M. Mench, J. Membr. Sci. 328 (2009) 113–120.
- [33] M. Khandelwal, S. Lee, M.M. Mench, J. Electrochim. Soc. 156 (2009) B703–B715.
- [34] J.H. Nam, K.-J. Lee, G.-S. Hwang, C.-J. Kim, M. Kavany, Int. J. Heat Mass Transfer 52 (2009) 2779–2791.
- [35] M.C. Leverett, Trans. AIME 142 (1941) 152–169.
- [36] E.C. Kumbur, K.V. Sharp, M.M. Mench, J. Power Sources 168 (2007) 356–368.
- [37] A. Çeçen, E.A. Wargo, A.C. Hanna, D.M. Turner, S.R. Kalidindi, E.C. Kumbur, J. Electrochim. Soc. 159 (2012) B299–B307.
- [38] E.A. Wargo, A.C. Hanna, A. Çeçen, S.R. Kalidindi, E.C. Kumbur, J. Power Sources 197 (2012) 168–179.
- [39] E.A. Wargo, V.P. Schulz, A. Çeçen, S.R. Kalidindi, E.C. Kumbur, Electrochim. Acta 87 (2013) 201–212.
- [40] J.T. Gostick, M.W. Fowler, M.A. Ioannidis, M.D. Pritzker, Y.M. Volfovich, A. Sakars, J. Power Sources 156 (2006) 375–387.
- [41] E.C. Kumbur, K.V. Sharp, M.M. Mench, J. Electrochim. Soc. 154 (2007) B1295–B1304.
- [42] E.C. Kumbur, K.V. Sharp, M.M. Mench, J. Electrochim. Soc. 154 (2007) B1305–B1314.
- [43] E.C. Kumbur, K.V. Sharp, M.M. Mench, J. Electrochim. Soc. 154 (2007) B1315–B1324.
- [44] Y.M. Volfovich, V.S. Bagotzky, V.E. Sosenkin, I.A. Blinov, Colloids Surf. A Physicochem. Eng. Asp. 187–188 (2001) 349–365.
- [45] J.P. Owejan, P. Nicotera, M.M. Mench, R.E. Evans, US Patent No. 8518596, USA, 2013.
- [46] K.S. Udell, Int. J. Heat Mass Transfer 28 (1985) 485–495.
- [47] A. Turhan, K. Heller, J.S. Brenizer, M.M. Mench, J. Power Sources 180 (2008) 773–783.
- [48] J.M. LaManna, S. Chakraborty, J.J. Gagliardo, M.M. Mench, Int. J. Hydrogen Energy 39 (2014) 3387–3396.
- [49] M.S. Ismail, T. Damjanovic, K. Hughes, D.B. Ingham, L. Ma, M. Pourkashanian, M. Rosli, J. Fuel Cell Sci Tech. 7 (2010) 051016–051016.
- [50] M.S. Ismail, D. Borman, T. Damjanovic, D.B. Ingham, M. Pourkashanian, Int. J. Hydrogen Energy 36 (2011) 10392–10402.